Onset of Coherent Oscillations in Turbulent Rayleigh-Bénard Convection

X.-L. Qiu and P. Tong*

Department of Physics, Oklahoma State University, Stillwater, Oklahoma 74078

(Received 2 May 2001; published 9 August 2001)

We report temperature cross correlation and velocity profile measurements in the aspect-ratio-one convection cell filled with water. A sharp transition from a random chaotic state to a correlated turbulent state of finite coherence time is found when the Rayleigh number becomes larger than a critical value $\mathrm{Ra}_c \simeq 5 \times 10^7$. The experiment reveals a unique mechanism for the onset of coherent oscillations in turbulent Rayleigh-Bénard convection.

DOI: 10.1103/PhysRevLett.87.094501 PACS numbers: 47.27.–i, 44.25.+f, 47.27.Te

Turbulent Rayleigh-Bénard convection is an interesting problem in nonlinear physics and has attracted much attention in recent years [1,2]. Despite its relatively low Reynolds number (Re), turbulent convection shares many common features that are usually associated with high Re turbulent flows. These features include coherent structures, intermittent fluctuations, and anomalous scaling. There are two coherent structures, which are found to coexist in the convection cell. One is the large-scale circulation that spans the height of the cell, and the other is intermittent bursts of thermal plumes from the upper and lower thermal boundary layers.

An intriguing feature of turbulent convection is the emergence of a well-defined oscillation frequency in the temperature [3,4] and velocity [5] power spectra at large Rayleigh numbers (Ra). While some arguments have been made to explain the coherent oscillation [3,4,6], its dynamic origin has remained elusive. Recently, Villermaux [7] proposed that this oscillation is caused by a thermal boundary layer instability triggered by the thermal plumes, which are transported along the cell periphery by the large-scale circulation. His model assumes that the unstable modes (i.e., the thermal plumes) in the upper and lower thermal boundary layers interact through a delayed nonlinear coupling with a time constant t_0. Because of this delayed coupling, the thermal plumes are excited alternately between the upper and lower boundary layers with a local frequency $f_0 \simeq 1/(2t_0)$. Villermaux's model provides an interesting mechanism for the coherent oscillation, but its predictions have not been examined experimentally in detail.

In this Letter, we report an experimental study of the coherent oscillation in turbulent Rayleigh-Bénard convection. A sharp transition from a random chaotic state to a correlated turbulent state of finite coherence time is found when Ra becomes larger than a critical value $\mathrm{Ra}_c \simeq 5 \times 10^7$. Above Ra_c the measured temperature cross-correlation function shows a well-defined oscillation with a finite coherence time. The experiment provides new insights into the physical understanding of the soft to hard turbulence transition [3,8], which occurs in the same Ra range.

The experiment is conducted in a cylindrical cell of aspect ratio one filled with water. Details about the apparatus have been described elsewhere [9], and here we mention only some key points. The upper and lower plates are made of brass and the sidewall is a transparent Plexiglas ring with a long rectangular flat window for the velocity measurement. Two Plexiglas rings of heights $H = 19.4$ and 8.2 cm are used to extend the accessible range of the Rayleigh number $\mathrm{Ra} = \alpha g H^3 \Delta T/(\nu\kappa)$, where ΔT is the temperature difference between the upper and lower surfaces, g is the gravitational acceleration, α, ν, and κ are, respectively, the thermal expansion coefficient, the kinematic viscosity, and the thermal diffusivity of the convecting fluid. In the experiment, the mean temperature of the bulk fluid is kept at $\sim$30 °C and the corresponding Prandtl number, $\mathrm{Pr} = \nu/\kappa$, is $\sim$5.4.

Two small movable thermistors are used to measure the local temperature of the convecting fluid. To guide the thermistors into the cell, we install two horizontal stainless steel tubes of diameter 1.1 mm on the opposite sides of the sidewall. The two tubes face each other and are mounted in such a way that the local fluid temperature $T_i(t)$ $(i = 1, 2)$ can be measured at various heights and horizontal positions away from the sidewall. Each thermistor is connected to an ac bridge as a resistance arm. The voltage signals from the two ac bridges are measured simultaneously by a two-channel dynamical signal analyzer (HP 35665A) at a sampling rate ranged from 2 to 20 Hz. Smaller sampling rates are used to obtain long time records (18–36 h) in order to achieve better statistics for the low-frequency data. All the thermistors are calibrated individually with an accuracy of 0.01 °C.

The velocity measurements are carried out using a two-component laser Doppler velocimeter (LDV) together with an argon ion laser. LDV measures the local velocity as a function of time and the velocity profile is obtained by scanning the velocity probe over an area of interest. It was found [5] that LDV is capable of measuring the flow velocity with high accuracy (better than 1%) over the entire cell, except near the upper and lower thermal boundary layers, whose thickness is of the order of 1 mm. In the boundary layer region, fluctuations of the fluid refractive

index due to strong temperature fluctuations reduce the signal-to-noise level of LDV.

Figure 1(a) shows the measured temperature cross-correlation function $g_c(\tau) = \langle \delta T_1(t) \delta T_2(t + \tau) \rangle / \Delta T^2$ as a function of delay time τ at three different values of Ra. Here the temperature fluctuation is defined as $\delta T_i(t) = T_i(t) - \bar{T}$, where $\bar{T}$ is the average local temperature. In the measurement, the two temperature probes are placed at the midheight of the cell and 8 mm away from each side of the sidewall; both of them are in the rotation plane of the large-scale circulation. Figure 1(a) reveals two important features of $g_c(\tau)$. First, the measured $g_c(\tau)$ has a well-defined oscillation at large Ra ($>\mathrm{Ra}_c \simeq 5 \times 10^7$). The oscillation frequency f_0 is found to vary with both H and Ra (see Fig. 2 below). Second, the measured $g_c(\tau)$ is a decaying function, indicating that the oscillation has a finite coherence time τ_c. The value of τ_c can be defined simply by counting how many oscillation cycles are in the measured $g_c(\tau)$. For example, we have $\tau_c f_0 \simeq 8$ at Ra $= 3.19 \times 10^9$.

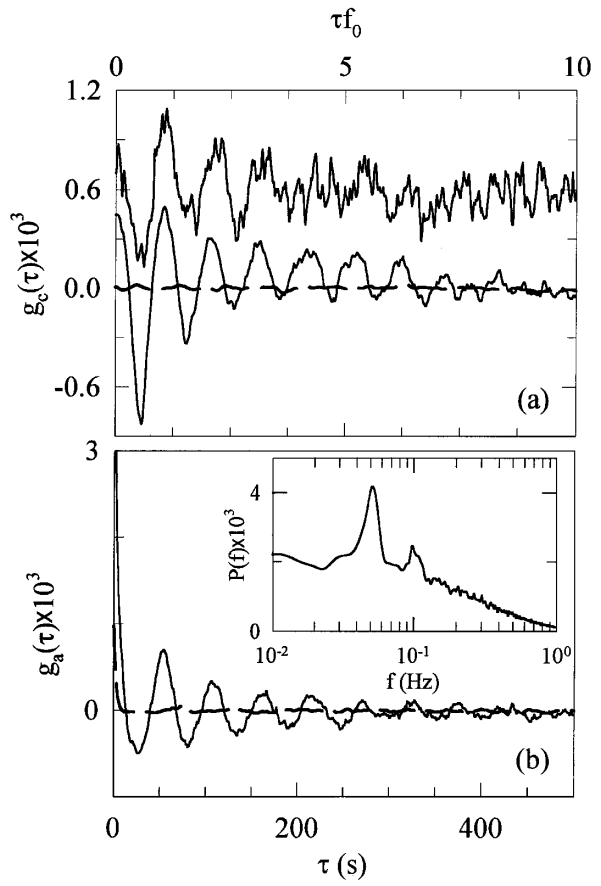

FIG. 1. (a) Measured temperature cross-correlation function $g_c(\tau)$ as a function of the normalized delay time τf_0 at Ra $= 3.19 \times 10^9$ (lower solid curve), 3.14×10^8 (upper solid curve), and 4.35×10^7 (dashed line). For clearness, the upper solid curve is shifted by 0.6×10^{-3}. (b) Measured temperature autocorrelation function $g_a(\tau)$ as a function of delay time τ at Ra $= 3.19 \times 10^9$ (solid curve) and 4.35×10^7 (dashed curve). Inset shows the frequency power spectrum $P(f)$ of the temperature signals at Ra $= 7.1 \times 10^8$.

These interesting features are also observed in the temperature autocorrelation function $g_a(\tau) = \langle \delta T_i(t) \delta T_i(t + \tau) \rangle / \Delta T^2$ ($i = 1$ or 2). Figure 1(b) shows the measured $g_a(\tau)$ at two different values of Ra. The measured $g_a(\tau)$ at Ra $= 3.19 \times 10^9$ has a decaying oscillatory form similar to that of $g_c(\tau)$. It is seen from Figs. 1(a) and 1(b) that the oscillations disappear from the measured $g_c(\tau)$ and $g_a(\tau)$ at small values of Ra ($<\mathrm{Ra}_c$).

The emergence of a well-defined oscillation in the near-wall region is an intriguing feature of turbulent convection and has stimulated considerable theoretical debates [3,4,6]. Villermaux's model [7] provides a detailed description for the coherent oscillation and gives two specific predictions, which can be compared with the experiment. Because of the alternating emission of the thermal plumes between the upper and lower thermal boundary layers, a local temperature probe will detect strong and weak burst signals in alternation. The strong signals, which come from the nearby conducting surface, contribute to a dominant peak at f_0 in the frequency power spectrum $P(f)$. The weak signals, on the other hand, are from the opposite conducting surface and give rise to a smaller harmonic peak at $2f_0$. Indeed, the measured $P(f)$ shown in the inset of Fig. 1(b) clearly reveals the second harmonic peak at $2f_0$. Figure 1(b) thus confirms the first prediction of Villermaux's model. Because of the limited frequency resolution, the second harmonic peak was not observed in early experiments [10].

Our recent velocity measurements [5,11] showed that the flow field in the aspect-ratio-one cell has a quasi-two-dimensional structure, which undergoes a coherent rotation. The single-roll structure can be divided into three regions in the rotation plane: (i) a thin viscous boundary layer around the cell boundary, (ii) a fully mixed central core region of size $\sim H/2$, and (iii) an intermediate plume-dominated buffer layer of thickness $\sim H/4$. The plume-dominated buffer layer is the active region that

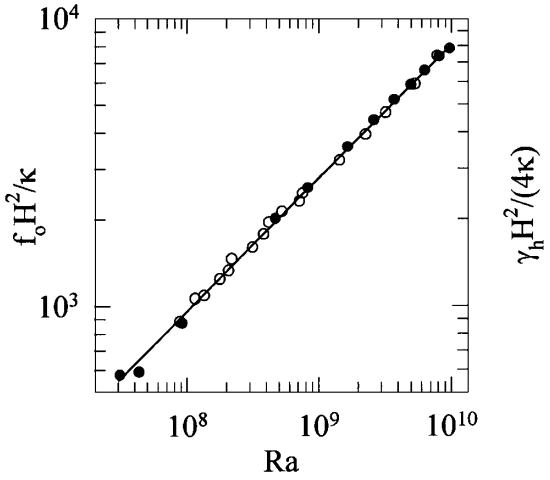

FIG. 2. Normalized oscillation frequency $f_0 H^2/\kappa$ (open circles) and plume traveling rate $\gamma_h H^2/(4\kappa)$ (closed circles) as a function of Ra. The solid line is a power-law fit to all the data points.

drives the large-scale coherent rotation (LSCR). Thermal plumes erupt into the region from the upper and lower thermal boundary layers and many of them are sheared to the sidewall region by the large-scale horizontal flow near the conducting surface. The warm and cold plumes, which are separated laterally in the two opposing sidewall regions, exert buoyancy forces on the fluid and drive the vertical flow near the sidewall. The central core region is "sheared" by the rising and falling plumes near the sidewall, resulting in a constant mean velocity gradient in the region.

It is found that at large Ra ($>\mathrm{Ra}_c$) the measured $g_c(\tau)$ shows oscillations only when both temperature probes are placed inside the plume-dominated buffer region. The oscillations disappear from $g_c(\tau)$ when one of the probes is moved out of the region. Inside the buffer region, maximum cross correlation is found when the two probes are placed at midheight on each side of the cell. In this case, one probe detects the rising warm plume and the other measures the falling cold plume. The two signals thus have a phase difference of 180°. The measured $g_c(\tau)$ at other locations in the buffer region is of the same shape as those shown in Fig. 1(a) but has a different initial phase. Their phase difference is consistent with the fact that the fluid moves up on one side of the cell and falls down on the opposite side of the cell.

With this flow structure, it becomes clear that the nonlinear delay time t_0 in Villermaux's model is the cell crossing time H/U, where U is the rising (or falling) speed of the thermal plumes. Therefore, we have $f_0 \simeq U/(2H)$. Figure 2 compares the measured $f_0 H^2/\kappa$ (open circles) with the normalized plume traveling rate $\gamma_h H^2/(4\kappa)$ (solid circles) for different values of Ra. Here γ_h is the rotation rate of LSCR and is obtained from the slope of the linear horizontal velocity profile (see the dashed line in Fig. 4). The plume speed is given by $U \simeq \gamma_h H/2$ and therefore we have $\gamma_h H^2/(4\kappa) \simeq (U/2H)H^2/\kappa$. Figure 2 thus confirms the second prediction of Villermaux's model.

For convection experiments in helium gas or mercury, direct velocity measurements are extremely difficult. The results shown in Fig. 2 thus provide an important connection between the temperature and velocity measurements. The solid line in Fig. 2 shows the power-law fit $0.20\mathrm{Ra}^{0.46}$ to all the data points. The fitted exponent is in good agreement with the previous measurements of $f_0 H^2/\kappa$ in other convecting fluids [3,4,6,12]. In many early experiments, however, f_0 was wrongly interpreted as the rotation frequency $U/(4H)$.

Figure 3 displays the normalized coherence time $\tau_c f_0$ as a function of Ra. It is clearly shown that the measured $\tau_c f_0$ undergoes a transition near $\mathrm{Ra}_c \simeq 5 \times 10^7$. Below Ra_c the measured $\tau_c f_0$ is zero and no obvious oscillation is found in $g_c(\tau)$. Above Ra_c the measured $g_c(\tau)$ starts to show oscillations and the coherence time τ_c increases sharply with Ra. At higher values of Ra ($>2 \times 10^9$), $\tau_c f_0$ becomes saturated at a constant value of ~ 8. This is a fascinating new effect, which was not discussed in Villermaux's model. The sharp transition for τ_c occurs in the same Ra range as that for the soft to hard turbulence transition [3,8]. While various gradual changes between the soft and the hard turbulence have been reported in early experiments [3,8,13], Fig. 3 reveals the most drastic change occurred near the transition. This is an important finding for the physical understanding of the universal behavior in the hard turbulence regime.

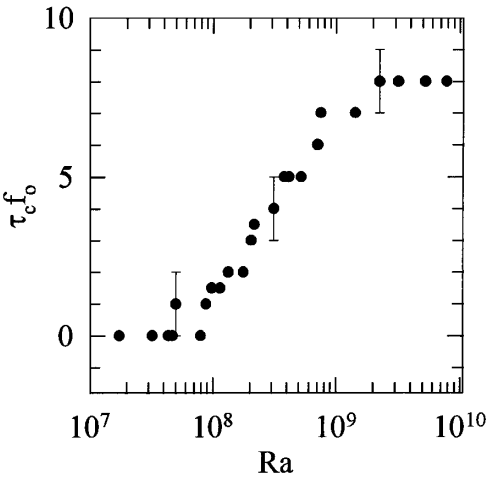

FIG. 3. Normalized coherence time $\tau_c f_0$ as a function of Ra.

To find how the coherence is generated, we measure the large-scale flow structure near the transition. Figure 4 compares the normalized horizontal velocity $u/u_{\max}$ (along the direction of the large-scale circulation) over varying vertical positions $\rho_z = z/H$ for three different values of Ra near Ra_c. The measurements are made along the central z axis from the lower surface ($\rho_z = 0$) to the upper surface ($\rho_z = 1$). It is seen that the measured velocity profiles at different Ra remain invariant and only $u_{\max}$ changes with Ra. Similar scaling behavior is also observed

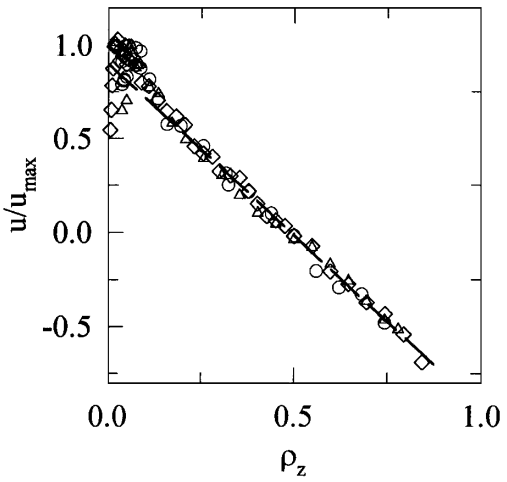

FIG. 4. Normalized horizontal velocity $u/u_{\max}$ as a function of the vertical position ρ_z. The measurements are made at $\mathrm{Ra} = 3.08 \times 10^7$ (circles), 9.14×10^7 (triangles), and 3.7×10^9 (diamonds). The dashed line is a linear fit to the data points in the central region of the cell.

for the horizontal velocity scan along the cell diameter at the midheight of the cell. The fact that the flow field still maintains a large-scale rotational structure below Ra_c suggests that LSCR provides only a means to transport the thermal plumes between the two conducting surfaces and is not sufficient to generate the coherent oscillation. Because of the random dephasing, coherent oscillation cannot occur if the rising (or falling) plumes arrive at the upper (or lower) surface randomly in time.

From the flow visualization at $Ra \simeq 10^9$, we observe that the thermal plumes in the sidewall region often group together when moving across the cell. Individual plumes are observed rarely near the sidewall. This collective behavior of the thermal plumes is also observed from the direct temperature measurement. Figure 5 shows the typical temperature fluctuations in the sidewall region at two different values of Ra; one is below Ra_c and the other is above Ra_c. Temperature fluctuations near the sidewall are found to be highly skewed toward one direction. Cold fluctuations are superposed on an average base line on one side of the cell and warm fluctuations are found on the opposite side of the cell. These upward going spikes are associated with the rising warm plumes in the sidewall region. A characteristic change shown in Fig. 5 is that below Ra_c the thermal plumes arrive individually at random time intervals [no peak is found in $P(f)$], whereas above Ra_c they arrive in groups at a frequency f_0 [a dominant peak at f_0 is found in $P(f)$]. Figure 5 thus suggests that the coherent oscillation is generated by a multiplume process involving many strongly interacting thermal plumes.

As shown in Fig. 1(b), the cell crossing time is $t_0 \simeq 28$ s at $Ra = 3.7 \times 10^9$. This time is too long for an individual rising plume of lifetime $t_1 \simeq \delta^2/\kappa$ to reach the upper surface. Here we take the thermal boundary layer thickness δ as the characteristic length (i.e., the thickness) of the plume. Using the experimental values $\delta \simeq 1$ mm and $\kappa \simeq 1.47 \times 10^{-3}$ cm^2/s, we have $t_1 \simeq 6.8$ s. This calculation suggests that above Ra_c the rising and falling plumes near the sidewall must be a new class of plumes, whose lifetime is longer than δ^2/κ. When two thermal plumes combine to form a "composite plume," the plume size is doubled and thus its lifetime is quadrupled. In this case, we have $t_2 \simeq (2\delta)^2/\kappa \simeq 27.2$ s, which is very close to the measured cell crossing time.

From the above measurements we conclude that at low Ra ($<Ra_c$), only a small number of thermal plumes are generated near the two conducting surfaces. These plumes erupt from the thermal boundary layers randomly and move independently in the cell. More plumes are generated as Ra is increased, and the system becomes "concentrated" when $Ra > Ra_c$. In this case, the thermal plumes interact strongly and their motion becomes correlated in time. The correlated motion provides synchronized stimulations, which are needed for the generation of the coherent oscillation. This is a self-feeding process involving multiple plumes under the influence of the large-scale rotation. Clearly, the experiment demonstrates how otherwise random unstable modes (i.e., the thermal plumes) in a closed cell are organized in both space and time to generate coherent oscillations in a turbulent environment.

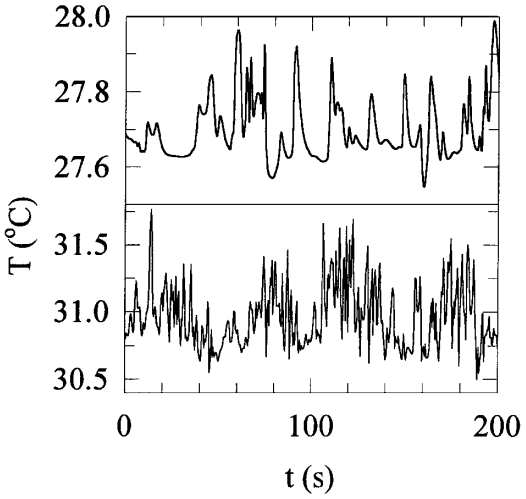

FIG. 5. Time series measurements of temperature fluctuations in the sidewall region at the midheight of the cell. The measurements are made at $Ra = 4.35 \times 10^7$ (upper curve) and 3.19×10^9 (lower curve).

We thank George Dixon and Xincheng Xie for useful discussions. The assistance of Mike Lucas and his team in fabricating the convection cell is gratefully acknowledged. This work was supported by the National Science Foundation under Grant No. DMR-0071323.

*Email address: ptong@okstate.edu

[1] E. Siggia, Annu. Rev. Fluid Mech. **26**, 137 (1994).
[2] S. Grossmann and D. Lohse, J. Fluid Mech. **407**, 27 (2000).
[3] B. Castaing, G. Gunaratne, F. Heslot, L. Kadanoff, A. Libchaber, S. Thomae, X.-Z. Wu, S. Zaleski, and G. Zanetti, J. Fluid Mech. **204**, 1 (1989).
[4] M. Sano, X.-Z. Wu, and A. Libchaber, Phys. Rev. A **40**, 6421 (1989).
[5] X.-L. Qiu, S.-H. Yao, and P. Tong, Phys. Rev. E **61**, R6075 (2000).
[6] S. Cioni, S. Ciliberto, and J. Sommeria, J. Fluid Mech. **335**, 111 (1997).
[7] E. Villermaux, Phys. Rev. Lett. **75**, 4618 (1995).
[8] F. Heslot, B. Castaing, and A. Libchaber, Phys. Rev. A **36**, 5870 (1987).
[9] Y.-B. Du and P. Tong, J. Fluid Mech. **407**, 57 (2000).
[10] In the fast Fourier transform (FFT), we use 1024 data points for each time record (256–512 s in length) and the result is averaged over 18–36 h. The frequency resolution of the FFT is thus $(1.95–3.9) \times 10^{-3}$ Hz.
[11] X.-L. Qiu and P. Tong, Phys. Rev. E (to be published).
[12] X. Chavanne, F. Chillà, B. Castaing, B. Hébral, B. Chabaud, and J. Chaussy, Phys. Rev. Lett. **79**, 3648 (1997).
[13] T. H. Solomon and J. P. Gollub, Phys. Rev. Lett. **64**, 2382 (1990); Phys. Rev. A **43**, 6683 (1991).